Hindawi
Shock and Vibration
Volume 2018, Article ID 6479480, 14 pages
https://doi.org/10.1155/2018/6479480

Research Article

Safety Evaluation of the Wear Life of High-Speed Railway Bridge Bearings by Monitoring Train-Induced Dynamic Displacements

Gaoxin Wang[1], **Youliang Ding**[2], **Hui Guo**[3] and **Xinxin Zhao**[3]

[1]*State Key Laboratory for Geomechanics and Deep Underground Engineering, China University of Mining and Technology, Xuzhou, China*
[2]*The Key Laboratory of Concrete and Prestressed Concrete Structures of Ministry of Education, Southeast University, Nanjing 210096, China*
[3]*Railway Engineering Research Institute, China Academy of Railway Sciences Corporation Limited, Beijing 100081, China*

Correspondence should be addressed to Youliang Ding; civilchina@hotmail.com

Received 22 June 2018; Revised 30 September 2018; Accepted 14 October 2018; Published 1 November 2018

Academic Editor: Mahdi Mohammadpour

Copyright © 2018 Gaoxin Wang et al. This is an open access article distributed under the Creative Commons Attribution License, which permits unrestricted use, distribution, and reproduction in any medium, provided the original work is properly cited.

Bridge bearings experience numerous small-amplitude displacements under environmental loads. The continuous cyclic accumulations of these small-amplitude displacements will result in severe wear on the poly-tetra-fluoro-ethylene (PTFE) plates in the bridge bearings, which seriously endangers the service life of bearings. Traditional method directly uses the linear wear rate of cumulative displacements in a short period to evaluate the wearing life, but the linear wear rate only in a short period such as several days may not represent the characteristics in the whole bridge service life. Hence, this research takes the spherical steel bearings of the Nanjing Dashengguan Yangtze River Bridge as a study object. The cumulative dynamic displacement (CDD) under the action of a single train and the cumulative bearing travel (CBT) under the continual actions of many trains are studied using the monitored longitudinal displacement data from spherical steel bearings. Furthermore, the probability statistics and the Monte Carlo sampling simulation for CDD are studied, and the safety evaluation method for bearing wear life in the real environment is proposed using a reliability index regarding the failure probability of monitored CBT over the wear limit during service lifetime. In addition, safety evaluation on the bearing wear life was performed to assess the condition of spherical steel bearings in the real service environment. The results can provide an important reference for analysis on the bearing wear life of long-span railway bridge structures.

1. Introduction

As the service time of railway bridges increases, some bridge components may suffer from the aging and damage problems due to the influence of external environment loads. Among these bridge components, the bridge bearing is an important load-bearing component in large-span railway bridge structures, which can suffer from a series of diseases, such as the disengagement of bearings, the uneven compression, the twisting and fracturing of the bearing plate, and the weld cracking, which directly threaten the safety of railway bridges [1–5]. For example, Wei et al. revealed that the fixed bearings of continuous high-speed railway bridges were vulnerable under earthquakes because they transferred most of the seismic forces between superstructure and piers, and the sliding friction action of fixed bearings can protect other components from severe damage under earthquakes [2]; the research results of Oh et al. showed that the rubber material characteristics and spherical shape of spherical elastomeric bearing were important parameters in reducing vibrations of railway bridge [3]; Huang et al. emphasized that bearing is the important part that connects the superstructure and substructure of a railway bridge, in which the occurrence of defects affects running safety [4]. Therefore, it is necessary to further study the bearing damage of high-speed railway bridges subjected to environmental loads to ensure safe operation.

Current research on bearing damage in high-speed railway bridges mainly concentrated on the following three aspects: (1) the causes of bearing damage and

prevention methods [4, 6, 7]. For example, Yan conducted a detailed study on the cause analysis and remediation measures for the roller bearings of the Sunkou Yellow River Bridge [7], and Huang et al. researched a rapid treatment technique for the damaged rocking axle bearing of a railway simply supported beam bridge [4]. (2) The damage recognition methods of bridge bearings [1, 8, 9]. For instance, Zhan et al. utilized the dynamic response of a bridge under an impact load to diagnose the bearing disengagement of existing rubber bearings [1]; Qiao conducted an in-depth study on a damage identification technique for bridge bearings based on the change rate of natural frequency [9]. (3) The influence of bearing damage on the mechanical properties of bridge structure [3,10–12]. For instance, one study revealed that the increased vibration level of a railway bridge could cause bridge bearing damage, and the rubber material characteristics and spherical shape were important parameters in reducing bridge vibration [3]; another study showed that the load-carrying fillet weld around the gusset plate of diagonal bracing at the bridge bearing was predicted to be the most fatigued critical detail among the various structural details, and a fatigue assessment was carried out for a composite railway bridge on which high-speed trains traveled [12].

The latest studies revealed that bridge bearings experienced numerous small-amplitude dynamic displacements under dynamic loads [13, 14]. Continuous accumulations of small-amplitude dynamic displacements can cause severe wear to poly-tetra-fluoro-ethylene (PTFE) plates of bridge bearings, which seriously decreases the service lifetime of bearings [13, 14]. For instance, according to the field results, the small but rapid girder movements contributed the most to the large cumulative movements, resulting in accelerated fatigue damage and bearing wear [13, 14]. However, current research mainly focuses on highway bridge bearings rather than railway bridge bearings. Large-span high-speed railway bridges have the special characteristics of being designed for high-speed trains. For example, the Dashengguan Yangtze River Bridge is one large-span steel truss arch bridge with a 336-meter-long main span and six tracks, and the designed high-speed train passed speed can reach 300 km/h [15]. These conditions can easily induce a large number of small-amplitude dynamic displacements, which can result in serious wear damage. However, current research has not clearly revealed the cumulative wear characteristics and the safety evaluation method for railway bridge bearings in the service lifetime.

Therefore, this research takes the spherical steel bearings of the Nanjing Dashengguan Yangtze River Bridge as a study object as shown in Figure 1 to investigate the cumulative dynamic displacement (CDD) under the action of a single train and the cumulative bearing travel (CBT) under the continual actions of many trains using monitored longitudinal displacement data of spherical steel bearings. Furthermore, the probability statistics and the Monte Carlo sampling simulation for CDD are studied, and the safety evaluation method for the bearing wear life is proposed using a reliability index regarding the failure probability of monitored CBT over the wear limit in the service lifetime. In addition, the safety evaluation for the bearing wear life was performed to assess the condition of spherical steel bearings in real service environment. Traditional method directly uses the linear wear rate of cumulative displacements in a short period to evaluate the wearing life, and such linear wear rate only in a short period such as several days may not represent the characteristics in the whole bridge service life, so the novelty of this paper is the safety evaluation method for the bearing wear life using a reliability index integrated with probability statistics analysis and Monte Carlo sampling simulation in the whole bridge life.

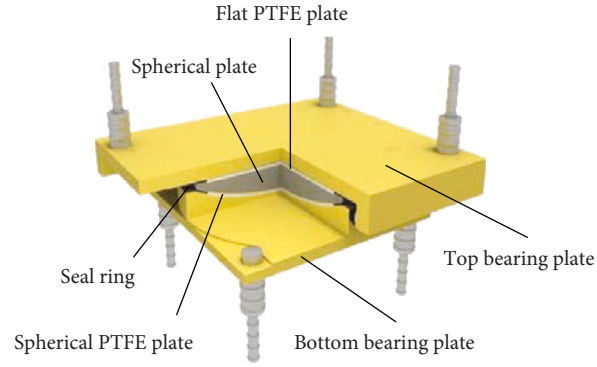

Figure 1: The components of spherical steel bearing.

2. Monitoring Data Analysis

2.1. Description of Bridge Health Monitoring. The Nanjing Dashengguan Yangtze River Bridge is a large-span high-speed railway steel truss arch bridge. It is designed for river crossing of the Beijing-Shanghai high-speed railway and the Shanghai-Wuhan-Chengdu high-speed railway, as shown in Figure 2. The upper structure of this bridge is a six-span continuous steel truss arch girder, which is composed of steel truss arch and steel bridge deck [16]. In detail, the steel truss arch is composed of chord members, diagonal web members, vertical web members, and horizontal and vertical bracings; the steel deck is composed of top plate and transverse stiffening girder. In addition, a total of seven groups of spherical steel bearings (i.e., bearings 1~7) are used to support the steel truss arch girder, where the bearing 4 is totally fixed in all the three translational directions while the other six bearings allow longitudinal thermal expansion in the steel truss arch girder.

Therefore, 12 LVDT displacement sensors (namely linear variable differential transformers) are installed at the upstream and downstream sides of the six groups of bearings (i.e., $B_{1,u}$~$B_{3,u}$, $B_{5,u}$~$B_{7,u}$, $B_{1,d}$~$B_{3,d}$, and $B_{5,d}$~$B_{7,d}$) for long-term monitoring of the longitudinal displacement data, where "u" indicates the upstream side, and "d" indicates the downstream side. In detail, the voltages in the displacement sensors which are termed as analog signals are amplified, filtered, and then transformed to the digital signals in the data acquisition station at bridge site, which can be remotely monitored, displayed, and downloaded through Internet in the health monitoring center far from

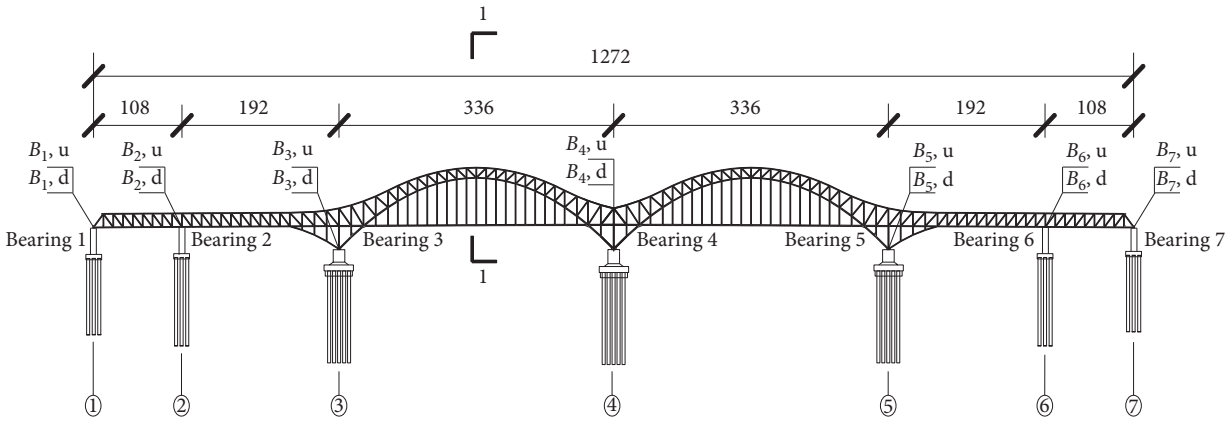

Figure 2: Locations of the longitudinal displacement sensors m.

the bridge site. The sampling frequency of the 12 displacement sensors is 1 Hz. Because the Nanjing Dashengguan Yangtze River Bridge is one symmetrical structure, only the bearings on the left half (i.e., $B_{1,u}$~$B_{3,u}$ and $B_{1,d}$~$B_{3,d}$) are selected for analysis.

2.2. Cumulative Dynamic Displacement Caused by a Passed Train. The monitored longitudinal displacement data at the ith spherical steel bearing $B_{i,u}$ are denoted by $D_{i,u}$; the monitored longitudinal displacement data at the ith spherical steel bearing $B_{i,d}$ are denoted by $D_{i,d}$; $i = 1, 2, 3$. Because the time histories of longitudinal displacements have similar change trends [16], only $D_{1,u}$ is selected for analysis. The time history of $D_{1,u}$ from March to October in 2017 is shown in Figure 3(a), showing typical seasonal characteristics over eight months. Furthermore, the time history of $D_{1,u}$ on May 20th, 2017 is plotted in Figure 3(b), showing typical sinusoidal characteristics. These variation characteristics are very similar to those of temperature field [17], indicating that the displacement is mainly induced by temperature field. In addition, Figure 3(b) shows the time history of $D_{1,u}$ from 16:00 to 18:00 on May 20th, 2017. It is clear that the longitudinal displacements contain numerous small-amplitude dynamic displacements with random variability that are mainly induced by dynamic loads.

Because the monitored longitudinal displacement data contain static longitudinal displacements induced by the temperature field and dynamic longitudinal displacements induced by dynamic loads as well, the dynamic longitudinal displacements need to be extracted from the monitored data first. Note that the static and dynamic longitudinal displacements are in different frequency bands. The static longitudinal displacement is greatly influenced by temperature changes, so the cycle period is about one day (i.e., the corresponding frequency is 1/86400 Hz). To ensure that the frequency of static longitudinal displacements is completely within the band range, the upper limit of the frequency band is designed to be 5/86400 Hz, namely (0, 5/86400] [13, 14]. The frequency of dynamic longitudinal displacements is far higher than the frequency of static longitudinal displacements, and relevant research has indicated that the frequency bandwidth of dynamic longitudinal displacements is within the range of (5/86400, 0.5] [13, 14]. The reason for choosing 0.5 Hz as the upper limit is that the dynamic displacements with frequencies over 0.5 Hz are mainly induced by electromagnetic interference [13, 14], which are not in the range of concern.

The wavelet packet decomposition method can use a pair of filters to decompose the monitored longitudinal displacement into different frequency bands scale by scale [18–20]. Figure 4 shows the tree structure of the wavelet packet coefficients within 13 scales after layer-by-layer decomposition, where $x_{j,m}$ denotes the wavelet packet coefficient in the mth frequency band of the jth scale ($m = 0, 1, 2, \ldots, 2^j - 1$), and f_s denotes the sampling frequency with $f_s = 1$ Hz in this research. The wavelet packet coefficient in the first frequency band $(0, 1/2^{14}]$, which is close to (0, 5/86400], is selected and reconstructed to obtain static displacements; the wavelet packet coefficients in the other frequency bands $(1/2^{14}, 1/2]$, which are close to (5/86400, 0.5], are selected and reconstructed to obtain dynamic displacements.

Taking Figure 3(b) as an example, the time history of $D_{1,u}$ on May 20th, 2017 is decomposed by the wavelet packet method, and the decomposition result is shown in Figure 5. It is clear that the wavelet packet decomposition method can effectively decompose the monitored longitudinal displacement data into two components: the first component caused by temperature field and the second component (namely small-amplitude dynamic displacements) caused by dynamic loads. Furthermore, the cumulative displacements of two components are calculated to investigate the contribution of two components to cumulative displacements, which are 47.1 mm and 773.4 mm, respectively. Obviously, the second component caused by dynamic loads contributes the most to cumulative displacements. In detail, the dynamic loads mainly include train and wind loads. What should be mentioned is that there is no train passing the Dashengguan Yangtze River Bridge from 0 am to 6 am for bridge inspection, so the first component during this period is mainly induced by wind load; in addition, the second component during the rest of time is mainly induced by both wind and train loads, as shown in Figure 5(b). It can be inferred from Figure 5(b) that train load is the major influence factor for cumulative displacements

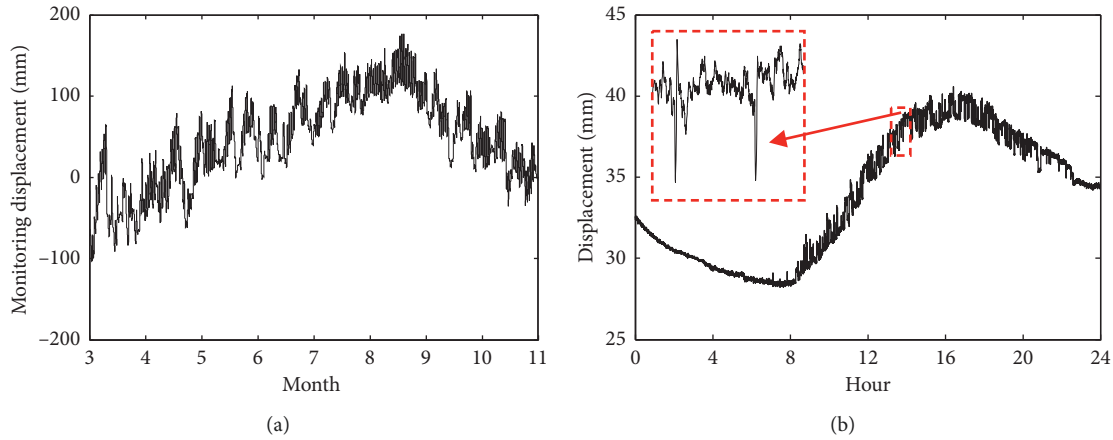

Figure 3: The monitored result of $D_{1,u}$. (a) From March to October in 2017. (b) On May 20th, 2017.

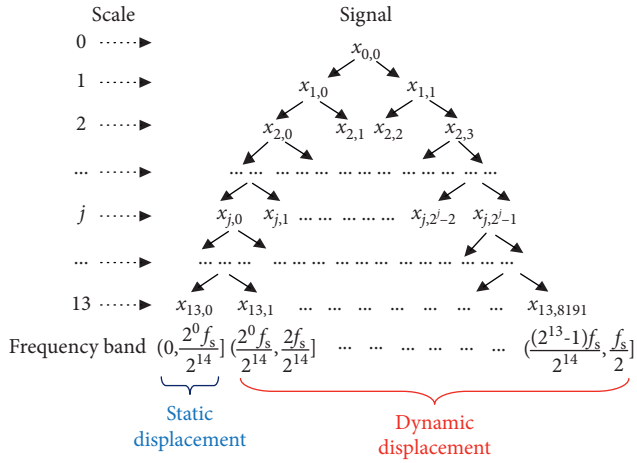

Figure 4: Tree structure of the wavelet packet coefficients.

because the influence of train load is obviously higher than wind load. Hence, the small-amplitude dynamic displacement caused by train load is specifically studied in this research.

The continuous accumulation of small-amplitude dynamic displacements will induce serious fatigue wear, which can severely decrease the service lifetime of bearings. Thus, it is necessary to carry out study on the cumulative characteristics of small-amplitude dynamic displacements. The CDD caused by a single passed train was calculated to evaluate the contribution of this train to the cumulative wear. The CDD caused by the kth passed train, which is denoted by $N(k)$, is calculated by referring to the equation in Table 1, where $\widetilde{D}(k)$ denotes the dynamic displacement caused by the kth passed train; $\widetilde{D}_j(k)$ and $\widetilde{D}_{j+1}(k)$ denote the jth and $(j+1)$th values in $\widetilde{D}(k)$, respectively, where $j = 1, 2, \ldots, U-1$; U denotes the number of monitored values in $\widetilde{D}(k)$. $N(k)$ indicates the cumulative travel of bearing caused by the kth passed train. For example, one time history of dynamic displacement of $B_{3,u}$ caused by one train is plotted in Figure 6, and the number of U in the train-passed segment of the plot is 48, which can be clearly captured, so the value of $N(k)$ is 20.3 mm by calculating the CDD in the train-passed segment.

The monitored data from August 10th to August 31st in 2017 is selected for analysis. A total of 3495 trains passed over the Dashengguan Yangtze River Bridge over this period, and each train corresponds to one value of $N(k)$. Therefore, 3495 values of $N(k)$ for each bearing at upstream and downstream sides (i.e., $B_{1,u}$~$B_{3,u}$ and $B_{1,d}$~$B_{3,d}$) are calculated as shown in Figure 7, where $N_{i,u}$ and $N_{i,d}$ denote a set of $\{N(1), N(2), \ldots, N(3495)\}$ for the bearings $B_{i,u}$ and $B_{i,d}$, respectively, as shown in Table 1. It can be seen that all the CDDs show uniform and random characteristics. Furthermore, the average value of 3495 CDDs for each $N_{i,u}$ or $N_{i,d}$, which is denoted by mean$(N_{i,u})$ or mean$(N_{i,d})$, respectively, is calculated by referring to the equations in Table 1, with the results shown in Figure 7. It can be seen that mean$(N_{3,d})$ has the largest value about 7.020 mm while mean$(N_{1,u})$ has the smallest value about 2.904 mm.

2.3. Cumulative Bearing Travel Caused by Many Passed Trains. Each value of $N_{i,u}$ or $N_{i,d}$ corresponds to one passed train, and furthermore, the 3495 values for each $B_{i,u}$ or $B_{i,d}$ are accumulated to obtain CBT, which indicates the influence of the continuous actions of passed trains on bearing wear. The calculation formula for CBT is expressed as follows:

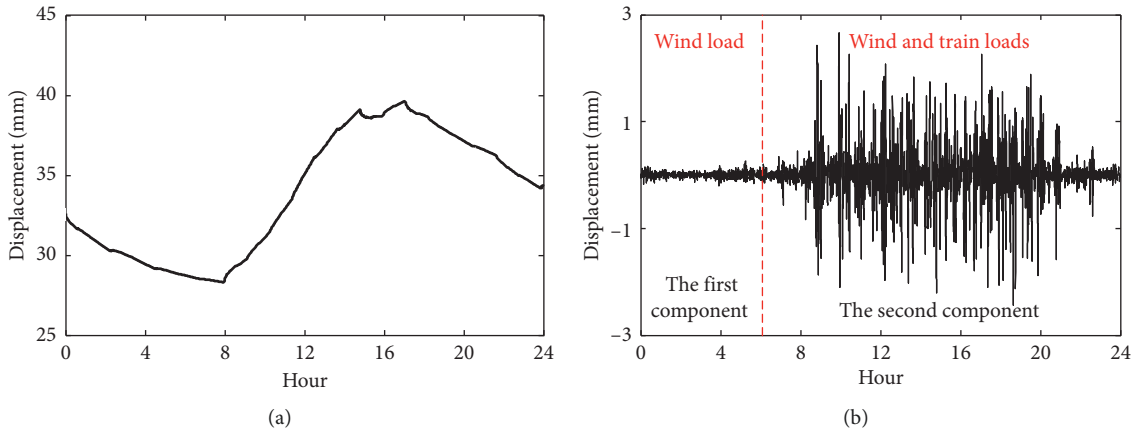

Figure 5: Decomposition result of monitored longitudinal displacement. (a) Component caused by temperature field. (b) Component caused by dynamical loads.

Table 1: Calculation of variables $N(k)$, $N_{i,u}$, $N_{i,d}$, mean$(N_{i,u})$, and mean$(N_{i,d})$.

Variable	Calculation equation
$N(k)$	$N(k) = \sum_{j=1}^{U-1} \lvert \tilde{D}_{j+1}(k) - \tilde{D}_j(k) \rvert$
$N_{i,u}$, $N_{i,d}$	$N_{i,u} = \{N(1), N(2), \ldots, N(3495)\}$ for the bearings at upstream $N_{i,d} = \{N(1), N(2), \ldots, N(3495)\}$ for the bearings at downstream
mean$(N_{i,u})$, mean$(N_{i,d})$	mean$(N_{i,u}) = (N(1) + N(2) + \cdots + N(3495)/3495)$ for the bearings at upstream mean$(N_{i,d}) = (N(1) + N(2) + \cdots + N(3495)/3495)$ for the bearings at downstream

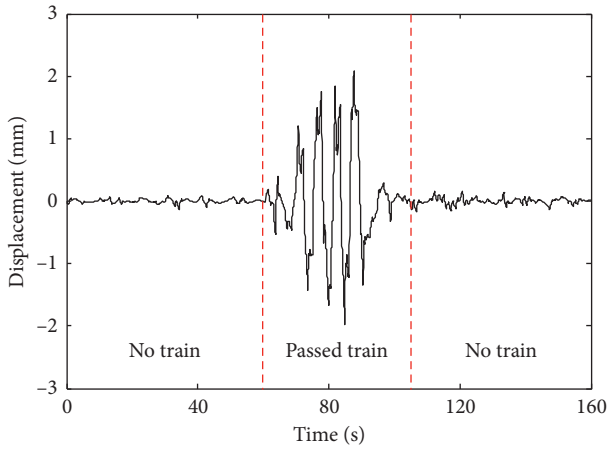

Figure 6: The dynamic displacement of $B_{3,u}$ caused by one train.

$$M(p) = \sum_{k=1}^{p} N(k), \tag{1}$$

where $M(p)$ denotes the CBT caused by p passed trains and $p = 1, 2, \ldots, 3495$. The $M(p)$ values at the upstream and downstream are shown in Figure 8, where $M_{i,u}$ denotes the CBT of $B_{i,u}$ and $M_{i,d}$ denotes the CBT of $B_{i,d}$ $(i = 1, 2, 3)$. It can be seen that all the CBTs have obvious linear correlations with the number of passed trains, but the linear growth rates are different for each $M_{i,u}$ or $M_{i,d}$, where the linear growth rate of $M_{3,d}$ is the fastest, and its maximum CBT caused by 3495 passed trains is 24360 mm.

3. Probability Statistics Analysis

The number of monitored CDDs are not enough to satisfy the requirement of large sample for safety evaluation of bearing wear life. Therefore, it is necessary to perform sampling simulation of CDDs using probabilistic statistics of the monitored CDDs to obtain adequate data.

3.1. Cumulative Probability Characteristics. Figure 7 shows that $N_{i,u}$ and $N_{i,d}$ contain obvious uniform and random characteristics, so $N_{i,u}$ and $N_{i,d}$ can be treated as statistical variables for probabilistic statistics analysis. In detail, the cumulative probability (CP) is used to describe the probabilistic statistics characteristics of CDDs. First, the cumulative probabilities of $N_{i,u}$ and $N_{i,d}$ are calculated based on probability statistics theory, and then the cumulative distribution function is fitted in a least-squares manner using the cumulative probabilities of $N_{i,u}$ and $N_{i,d}$, which is illustrated in two steps as follows:

(1) The cumulative probabilities of $N_{i,u}$ and $N_{i,d}$ are calculated as follows:

$$P\left(N_{i,u}(j)\right) = \frac{\mathrm{NUM}\left(N_{i,u} < N_{i,u}(j)\right)}{\mathrm{NUM}\left(N_{i,u}\right)}, \tag{2a}$$

$$P\left(N_{i,d}(j)\right) = \frac{\mathrm{NUM}\left(N_{i,d} < N_{i,d}(j)\right)}{\mathrm{NUM}\left(N_{i,d}\right)}, \tag{2b}$$

where $P(N_{i,u}(j))$ denotes the CP of the jth value $N_{i,u}(j)$ in $N_{i,u}$; $P(N_{i,d}(j))$ denotes the CP of the jth

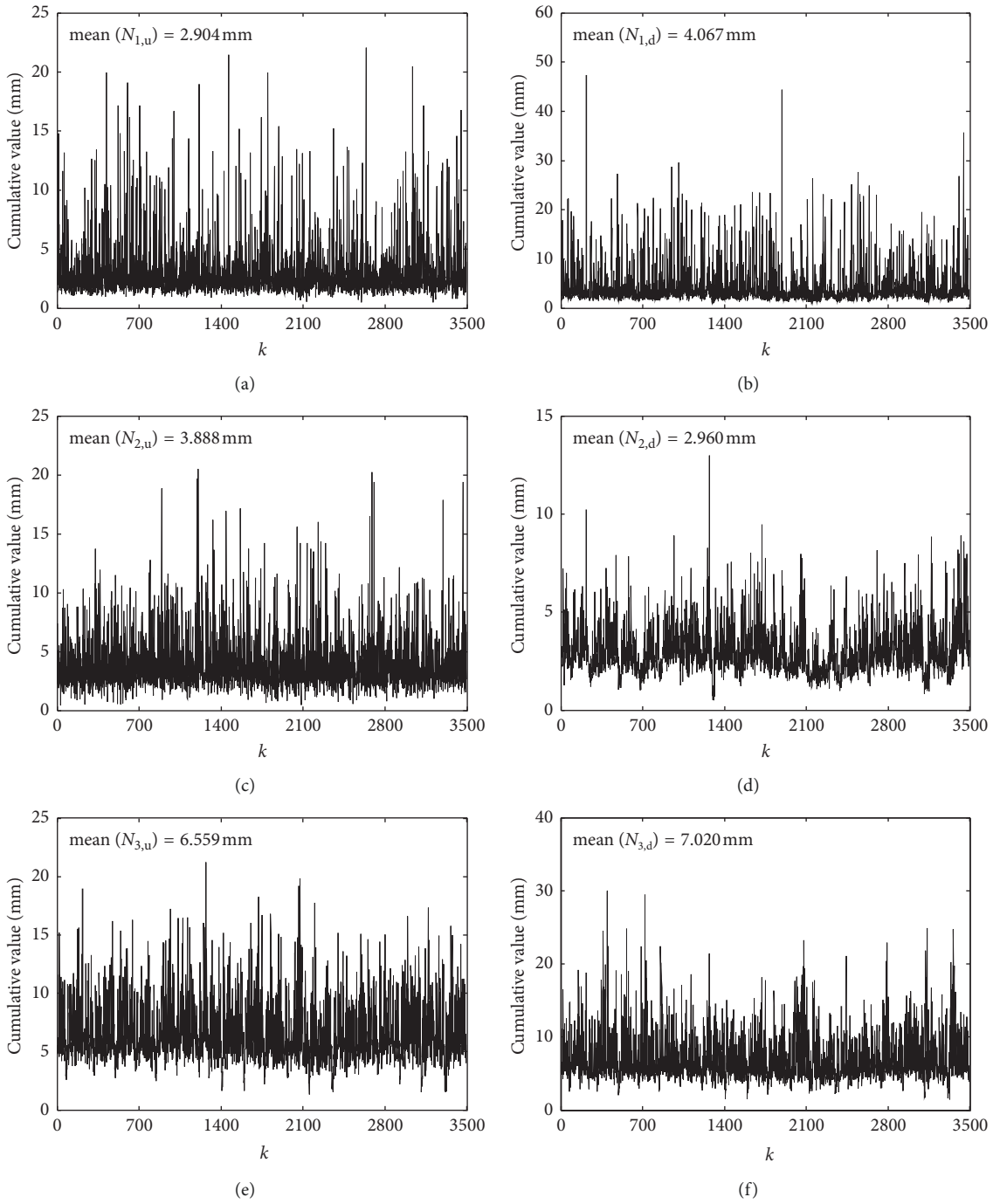

FIGURE 7: $N_{i,u}$ and $N_{i,d}$. (a) $N_{1,u}$. (b) $N_{1,d}$. (c) $N_{2,u}$. (d) $N_{2,d}$. (e) $N_{3,u}$. (f) $N_{3,d}$.

value $N_{i,d}(j)$ in $N_{i,d}$; NUM($N_{i,u}$) denotes the total number of $N_{i,u}$; NUM($N_{i,d}$) denotes the total number of $N_{i,d}$; NUM($N_{i,u} < N_{i,u}(j)$) denotes the number of CDDs in $N_{i,u}$ that are smaller than $N_{i,u}(j)$; and NUM($N_{i,d} < N_{i,d}(j)$) denotes the number of CDDs in $N_{i,d}$ that are smaller than $N_{i,d}(j)$. For instance, the CP of $N_{1,u}$ is shown in Figure 9.

(2) The cumulative distribution function is fitted in a least-squares manner using the cumulative probabilities of $N_{i,u}$ and $N_{i,d}$. Considering that the true cumulative distribution function of $N_{i,u}$ and $N_{i,d}$ is unknown, three possible cumulative distribution functions (i.e., normal distribution (ND), Weibull distribution (WD), and general extreme value distribution (GEVD)) are chosen for least-square fitting, and then the cumulative distribution function with the best fitting effect is selected as the true cumulative distribution function of $N_{i,u}$ and $N_{i,d}$. Taking $N_{1,u}$ as an example, the fitting results of the three cumulative

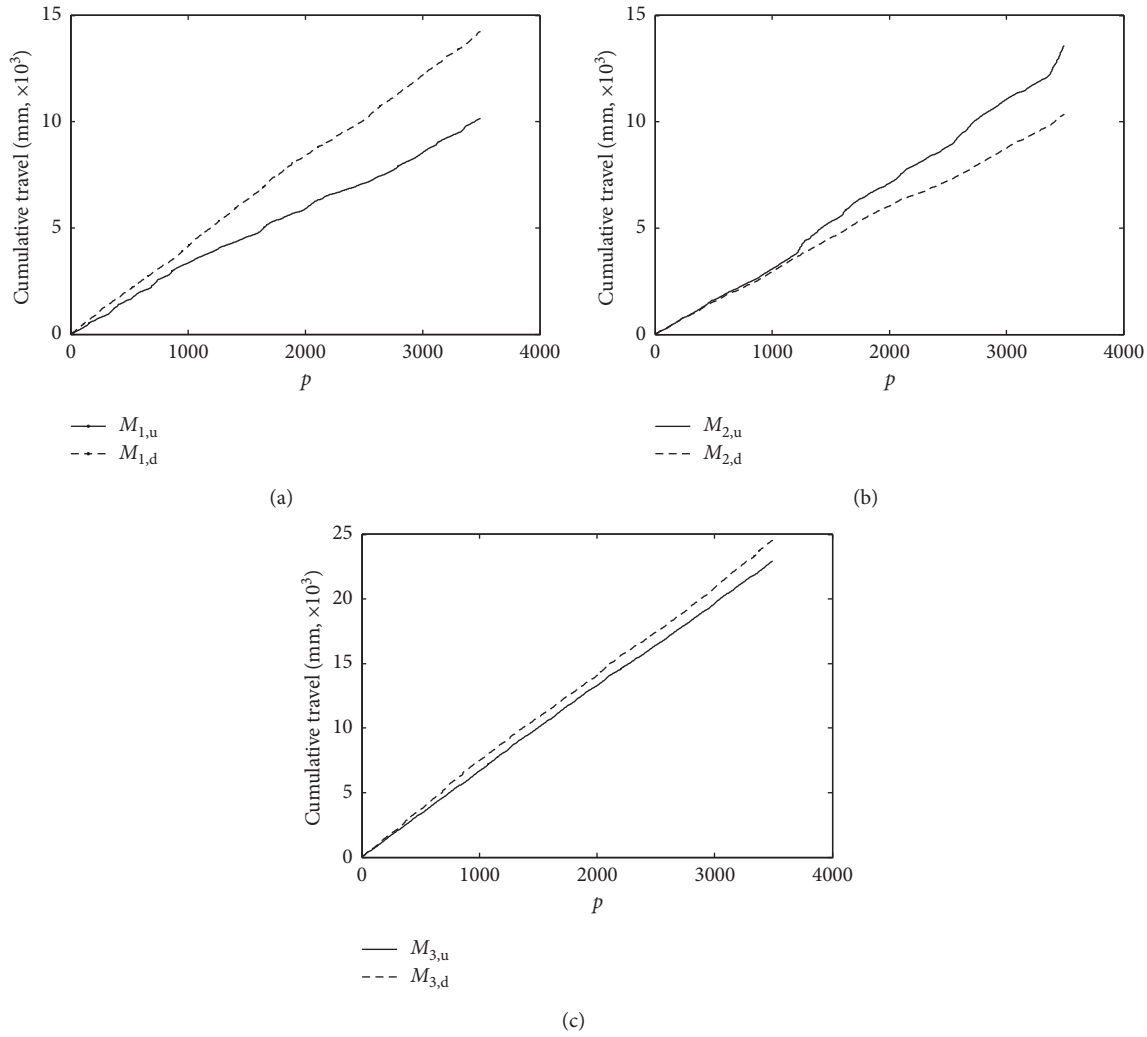

Figure 8: The $M_{1,u} - M_{3,u}$ and $M_{1,u} - M_{3,u}$ caused by many passed trains. (a) $M_{1,u}$ and $M_{1,d}$. (b) $M_{2,u}$ and $M_{2,d}$. (c) $M_{3,u}$ and $M_{3,d}$.

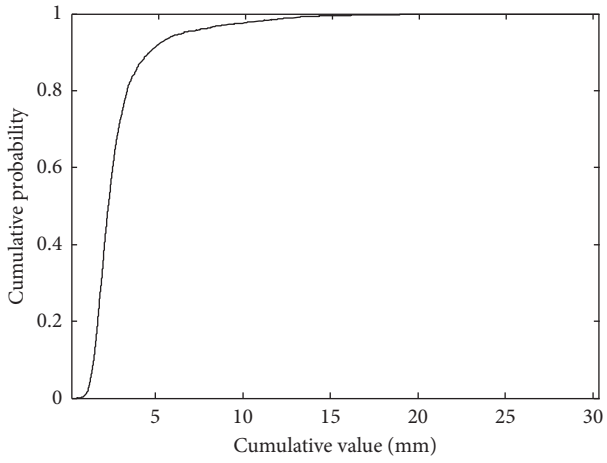

Figure 9: The cumulative probability of $N_{1,u}$.

distribution functions are shown in Figure 10. It can be seen that GEVD has the best fitting results, so GEVD is chosen to describe the cumulative probability characteristics of $N_{1,u}$. The formula is expressed as

$$G\left(N_{1,u}\right) = \exp\left[-\left[1 + r\left(\frac{N_{1,u} - b}{a}\right)\right]^{-1/r}\right], \quad (3)$$

where $G(N_{1,u})$ denotes the cumulative distribution function of $N_{1,u}$, which follows the generalized extreme value distribution; r denotes the shape parameter; a denotes the scale parameter; and b denotes the location parameter. The fitted values of these three parameters for $G(N_{1,u})$ are $r = 0.3058$, $a = 0.8163$, and $b = 2.0294$.

Based on the method above, the best cumulative distribution functions of $N_{1,u} - N_{3,u}$ and $N_{1,d} - N_{3,d}$ are all GEVD, as shown in Figures 10(a)–10(f). It can be seen that GEVD can well describe the cumulative probability characteristics of $N_{1,u} - N_{3,u}$ and $N_{1,d} - N_{3,d}$.

3.2. Sampling Simulation Method. Since $N_{i,u}$ and $N_{i,d}$ follow GEVDs, their GEVDs can be utilized for Monte Carlo sampling to obtain a demanded number of CDDs. Specifically, if the demanded number of CDDs is K, K values are

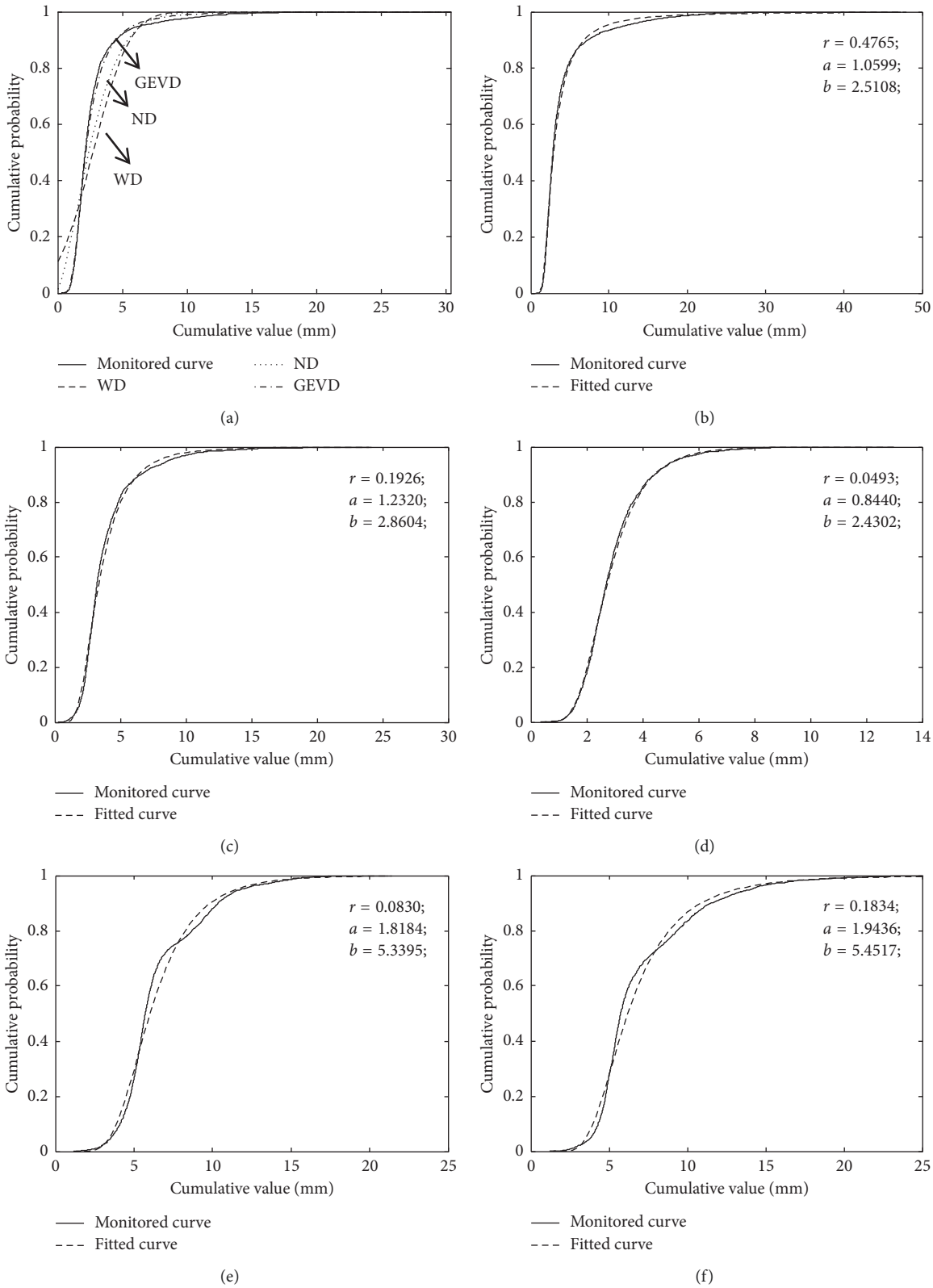

Figure 10: GEVDs of $N_{1,u} - N_{6,u}$ and $N_{1,u} - N_{6,u}$. (a) $N_{1,u}$. (b) $N_{1,d}$. (c) $N_{2,u}$. (d) $N_{2,d}$. (e) $N_{3,u}$. (f) $N_{3,d}$.

uniformly and randomly sampled from the interval (0, 1), and then the demanded number of CDDs can be simulated by substituting the K values into the cumulative probability R in the following equations:

$$R = G\left(N_{i,\mathrm{us}}\right), \tag{4a}$$

$$R = G\left(N_{i,\mathrm{ds}}\right), \tag{4b}$$

$$G\left(N_{i,\mathrm{us}}\right) = \exp\left[-\left[1 + r\left(\frac{N_{i,\mathrm{us}} - b}{a}\right)\right]^{-1/r}\right], \tag{4c}$$

$$G\left(N_{i,\mathrm{ds}}\right) = \exp\left[-\left[1 + r\left(\frac{N_{i,\mathrm{ds}} - b}{a}\right)\right]^{-1/r}\right], \tag{4d}$$

where $N_{i,\mathrm{us}}$ and $N_{i,\mathrm{ds}}$ denote the simulated CDDs of $N_{i,\mathrm{u}}$ and $N_{i,\mathrm{d}}$, respectively. The values of r, a, and b have been calculated in the Section 3.2. However, $N_{i,\mathrm{u}}$ and $N_{i,\mathrm{d}}$ are embedded in $G(N_{i,\mathrm{u}})$ and $G(N_{i,\mathrm{ds}})$, so they cannot be directly solved from Equations (4a) and (4b). Considering that $G(N_{i,\mathrm{us}})$ and $G(N_{i,\mathrm{ds}})$ are monotonically increasing functions, $N_{i,\mathrm{us}}$ and $N_{i,\mathrm{ds}}$ can be determined by the Newton iteration method as follows:

$$N_{i,\mathrm{us}}^{n+1} = N_{i,\mathrm{us}}^{n} - \frac{G\left(N_{i,\mathrm{us}}^{n}\right) - R}{G'\left(N_{i,\mathrm{us}}^{n}\right)}, \tag{5a}$$

$$N_{i,\mathrm{ds}}^{n+1} = N_{i,\mathrm{ds}}^{n} - \frac{G\left(N_{i,\mathrm{ds}}^{n}\right) - R}{G'\left(N_{i,\mathrm{ds}}^{n}\right)}, \tag{5b}$$

where $N_{i,\mathrm{us}}^{n+1}$ and $N_{i,\mathrm{us}}^{n}$ denote the $(n+1)$th and nth iteration results of $N_{i,\mathrm{us}}$, respectively; $N_{i,\mathrm{ds}}^{n+1}$ and $N_{i,\mathrm{ds}}^{n}$ denote the $(n+1)$th and nth iteration results of $N_{i,\mathrm{ds}}$, respectively; $G'(N_{i,\mathrm{us}}^{n})$ and $G'(N_{i,\mathrm{ds}}^{n})$ denote the first-order derivatives of GEVD (i.e., the probability density functions of GEVD). The iteration will terminate when the absolute difference between two adjacent iterations is less than 10^{-2}. The last iteration result is treated as the values of $N_{i,\mathrm{us}}$ and $N_{i,\mathrm{ds}}$.

3.3. The Sampling Simulation Result. Based on the sampling simulation method above, the simulation results of 3495 $N_{1,\mathrm{us}}$ are shown in Figure 11(a). The mean value of the simulated result is 2.820 mm, which is very close to the mean value of $N_{i,\mathrm{u}}$, i.e., 2.904 mm. Furthermore, the CP of the simulated result is calculated and then compared with the monitored CP, as shown in Figure 11(b). It can be seen that the simulated CP coincides with the monitored CP, which verifies the accuracy of the sampling simulation method.

Furthermore, the simulated 3495 values of $N_{i,\mathrm{us}}$ and $N_{i,\mathrm{ds}}$ are accumulated using Equation (1) to obtain the simulated CBT (i.e., $M_{i,\mathrm{us}}$ and $M_{i,\mathrm{ds}}$) as shown in Figure 12. It can be seen that the simulated $M_{i,\mathrm{us}}$ and $M_{i,\mathrm{ds}}$ present good linear growth characteristics with the number of passed trains. To verify the accuracy of the simulated linear growth rates, a comparison between the monitored and simulated linear growth rates was conducted as shown in Figure 12. It can be seen that the simulated linear growth rates have agreement with the monitored ones, which further verifies the accuracy of the sampling simulation method.

4. Safety Evaluation Analysis

The CBT relates to the bearing wear condition. If the CBTs exceed the wear limit in the service lifetime, the spherical steel bearing is totally damaged and cannot be used for longitudinal thermal expansion any longer. Therefore, it is necessary to analyze whether the CBTs at bridge site can exceed the wear limit in the service lifetime.

4.1. Evaluation Method. The failure probabilities of spherical steel bearings in the service lifetime (i.e., the probabilities of CBT over the wear limit in the service lifetime) are calculated as follows:

$$P_{\mathrm{f}} = 1 - F\left(\left[M_{i,\mathrm{us}}\right]\right) = P\left(M_{i,\mathrm{us}} > \left[M_{i,\mathrm{us}}\right]\right), \tag{6a}$$

or

$$P_{\mathrm{f}} = 1 - F\left(\left[M_{i,\mathrm{ds}}\right]\right) = P\left(M_{i,\mathrm{ds}} > \left[M_{i,\mathrm{ds}}\right]\right), \tag{6b}$$

$$M_{i,\mathrm{us}} = \sum_{j=1}^{J} N_{i,\mathrm{us}}(j), \tag{6c}$$

$$M_{i,\mathrm{ds}} = \sum_{j=1}^{J} N_{i,\mathrm{ds}}(j), \tag{6d}$$

where P_{f} denotes the failure probability; $[M_{i,\mathrm{us}}]$ and $[M_{i,\mathrm{ds}}]$ denote the wear limits of $B_{i,\mathrm{u}}$ and $B_{i,\mathrm{d}}$, respectively; $F([M_{i,\mathrm{us}}])$ and $F([M_{i,\mathrm{ds}}])$ denote the cumulative distribution functions with assigned values $[M_{i,\mathrm{us}}]$ and $[M_{i,\mathrm{ds}}]$, respectively, namely, $F(M_{i,\mathrm{us}} = [M_{i,\mathrm{us}}])$ and $F(M_{i,\mathrm{ds}} = [M_{i,\mathrm{ds}}])$; $N_{i,\mathrm{us}}(j)$ and $N_{i,\mathrm{ds}}(j)$ denote the jth values of $N_{i,\mathrm{us}}$ and $N_{i,\mathrm{ds}}$ in the service lifetime, respectively, which can be obtained through sampling simulation as introduced in the Section 3.2; and J denotes the total number of passed trains in the service lifetime.

$F(M_{i,\mathrm{us}})$ and $F(M_{i,\mathrm{us}})$ are unknown, which should be first determined by the following two steps:

(1) By referring to the sampling simulation method in the Section 3.2, the values of $N_{i,\mathrm{us}}$ or $N_{i,\mathrm{ds}}$ in the service life are simulated through Monte Carlo sampling. Then, the values of $N_{i,\mathrm{us}}$ or $N_{i,\mathrm{ds}}$ are summed using Equation (6c) or (6d), respectively, to obtain one value of $M_{i,\mathrm{us}}$ or $M_{i,\mathrm{ds}}$. This step is repeated W times to obtain W values of $M_{i,\mathrm{us}}$ or $M_{i,\mathrm{ds}}$;

(2) The cumulative probability characteristics for the W values of $M_{i,\mathrm{us}}$ or $M_{i,\mathrm{ds}}$ are fitted using cumulative distribution function. The true cumulative distribution function of $M_{i,\mathrm{us}}$ and $M_{i,\mathrm{ds}}$ is unknown, so three possible cumulative distribution functions (namely, ND, WD, and GEVD) are considered, and the cumulative distribution function with the best fitting effect is selected as the true cumulative

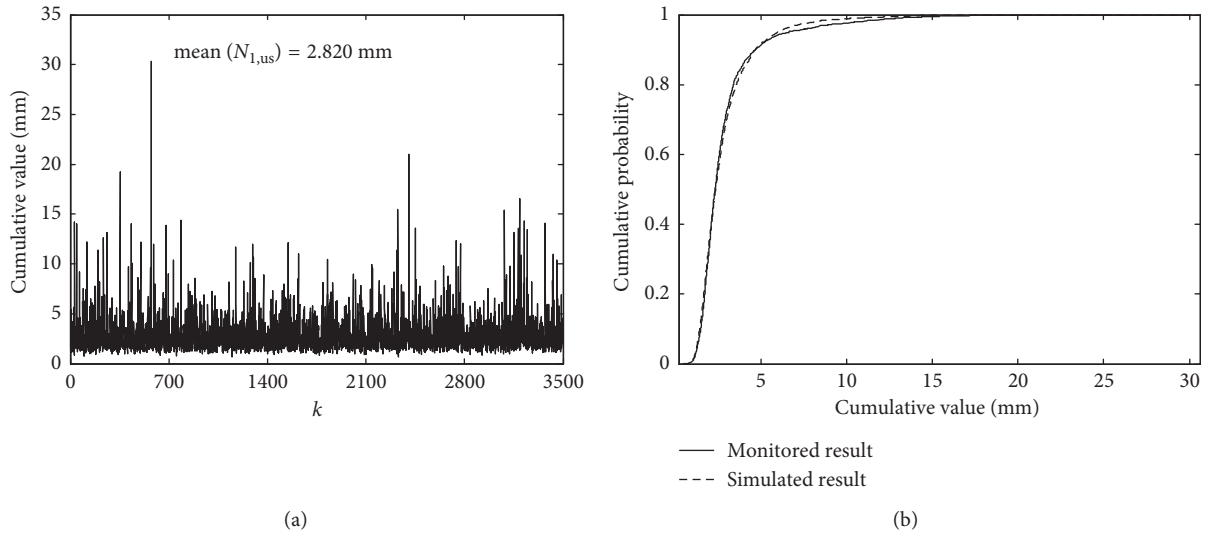

Figure 11: The simulated $N_{1,us}$ and its CP. (a) The simulated result. (b) A comparison between the simulated and monitored results.

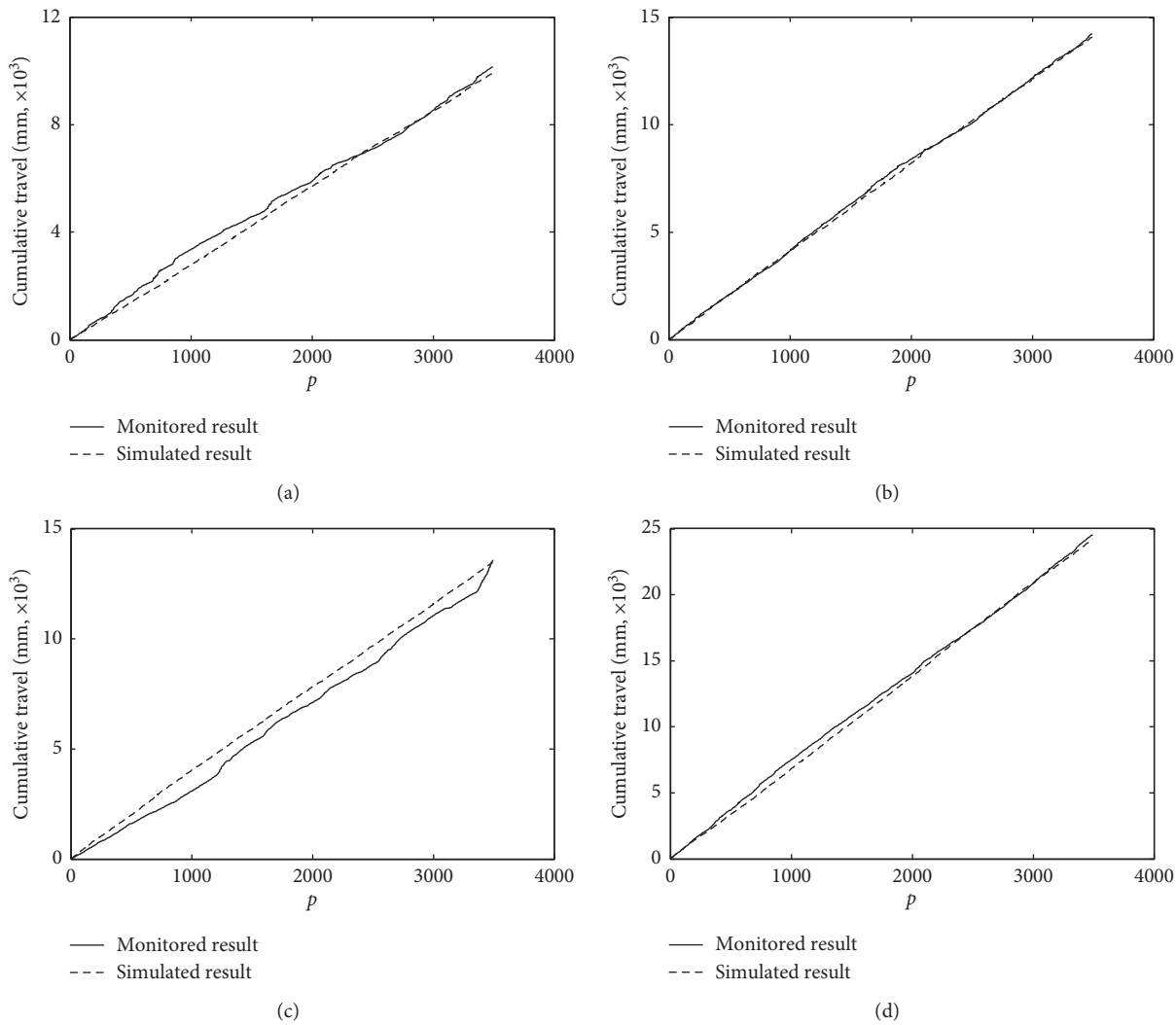

Figure 12: Continued.

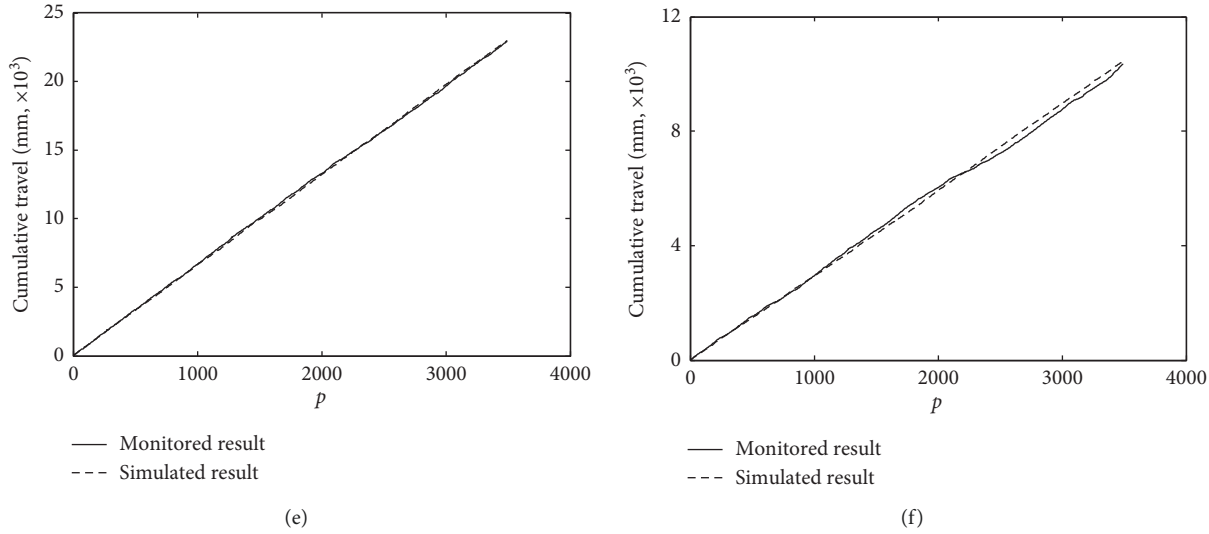

FIGURE 12: The simulated $M_{i,\mathrm{us}}$ and $M_{i,\mathrm{ds}}$. (a) $M_{1,\mathrm{us}}$ and $M_{1,\mathrm{u}}$. (b) $M_{1,\mathrm{ds}}$ and $M_{1,\mathrm{d}}$. (c) $M_{2,\mathrm{us}}$ and $M_{2,\mathrm{u}}$. (d) $M_{2,\mathrm{ds}}$ and $M_{2,\mathrm{d}}$. (e) $M_{3,\mathrm{us}}$ and $M_{3,\mathrm{u}}$. (f) $M_{3,\mathrm{ds}}$ and $M_{3,\mathrm{d}}$.

distribution function of $M_{i,\mathrm{us}}$ and $M_{i,\mathrm{ds}}$ after least-square fitting.

After $F(M_{i,\mathrm{us}})$ and $F(M_{i,\mathrm{us}})$ are determined, $[M_{i,\mathrm{us}}]$ and $[M_{i,\mathrm{ds}}]$ are substituted in Equations (6a) and (6b) to obtain the value of P_f. Furthermore, the reliability level β can be calculated using P_f as follows:

$$P_\mathrm{f} = \int_{\beta}^{+\infty} \frac{1}{\sqrt{2\pi}} \mathrm{e}^{-x^2/2}\, dx. \tag{7}$$

If the calculated reliability level β is larger than the target reliability level $[\beta]$ (i.e., $\beta > [\beta]$), it can be inferred that the bearing is still in a good service state; otherwise (i.e., $\beta \le [\beta]$), it can be inferred that the bearing is in a poor service state and should be replaced in time. According to the Eurocode [21], the target reliability level $[\beta]$ for newly built bridges with a 100-year design lifetime is 3.8, which corresponds to a failure probability $P_\mathrm{f} = 7.2 \times 10^{-5}$. However, the Dashengguan Railway Bridge has been in operation for 8 years, and it is not a newly built bridge. From the viewpoint of bridge reliability, a reduction in the uncertainties of the load and resistance parameters decreases the failure probability of existing bridge structures, indicating the possibility of adopting a lower reliability level for the evaluation of existing bridges rather than the reliability level that should be used for newly built bridges [22]. According to Kotes' research [22], the target reliability level $[\beta]$ with a 90-year remaining lifetime is 3.773, so the target reliability level $[\beta]$ of the Dashengguan Railway Bridge with a 92-year remaining lifetime is 3.778 using the linear interpolation calculation, namely, $[\beta] = 3.778$.

4.2. Evaluation Results. Figure 8 reveals that $M_{3,\mathrm{d}}$ has the fastest growth, so $M_{3,\mathrm{d}}$ is taken as an example to calculate its failure probability and evaluate the wear condition of $B_{3,\mathrm{d}}$ in the service lifetime. Before evaluation, three parameters should be determined, namely, J, $[M_{3,\mathrm{ds}}]$, and W. For the parameter J, the designed service life of the Nanjing Dashengguan Yangtze River Bridge is 100 years, and the number of passed trains in 2017 was 84343, so the value of J is 8434300; for the parameter $[M_{3,\mathrm{ds}}]$, the China code specifies that the linear wear rate of PTFE in a spherical steel bearing should be less than 15 μm/km and that the thickness of PTFE should be more than 7 mm and less than 8 mm (i.e., only a 1 mm wear thickness is allowed for an 8 mm thickness of PTFE) [23], so the value of $[M_{3,\mathrm{ds}}]$ is 66.7 km for the spherical steel bearing; for the parameter W, a larger W can provide better evaluation results, and the value of W is 1000 for evaluation in this research.

After the three parameters are determined, the bearing wear life is evaluated by the following seven steps:

(1) The values of $N_{3,\mathrm{d}}$ in 100-year service life are simulated through Monte Carlo simulation using Equation (4b), and 8434300 values of $N_{3,\mathrm{ds}}$ are obtained.

(2) All the 8434300 values of $N_{3,\mathrm{ds}}$ are summed to obtain the $M_{3,\mathrm{ds}}$ of $B_{3,\mathrm{d}}$ in 100-year service life using Equation (6d).

(3) Steps (1) and (2) are repeated 1000 times to obtain 1000 values of $M_{3,\mathrm{ds}}$, as shown in Figure 13(a). The 1000 values of $M_{3,\mathrm{ds}}$ show good uniform and random characteristics, and these values can be used to analyze the cumulative probability characteristics.

(4) The cumulative probability of $M_{3,\mathrm{ds}}$ is calculated and fitted by the ND, WD, and GEVD, with the fitted results shown in Figure 13(b). Both the ND and GEVD can well describe the cumulative probability characteristics of $M_{3,\mathrm{ds}}$, and GEVD is chosen for the true cumulative distribution function of $M_{3,\mathrm{ds}}$.

(5) The failure probability P_f of CBT over the upper limit $[M_{3,\mathrm{ds}}]$ for bearing $B_{3,\mathrm{d}}$ is about 10^{-8} calculated by

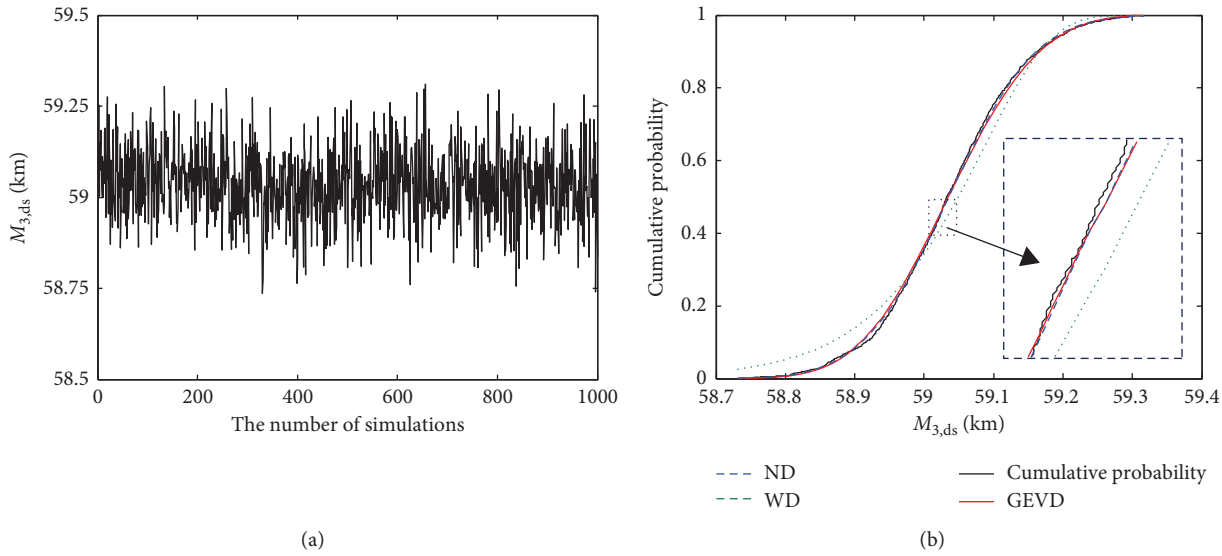

FIGURE 13: The 1000 values of $M_{3,ds}$ and their cumulative probabilities. (a)1000$M_{3,ds}$. (b) Cumulative probability of $M_{3,ds}$ and its fitted results.

Equation (6b), which means that $M_{3,ds}$ has little probability of exceeding $[M_{3,ds}]$ because the simulated 1000 values of $M_{3,ds}$ are within a small interval [58.74 km, 59.31 km].

(6) The reliability level β is 5.612 calculated by Equation (7), which is larger than the target reliability level 3.778, indicating that bearing $B_{3,d}$ does not reach the wear limit in the service life.

(7) Because the linear growth rate of CBT for $B_{3,d}$ is faster than those of the other spherical steel bearings, it can be inferred that the other spherical steel bearings do not reach the wear limit as well in the service life.

5. Conclusions

Based on the monitored dynamic displacement data of steel truss arch bridge bearings, the CDD under the action of a single train and the CBT under the continual actions of many passed trains are investigated. Furthermore, the probability statistics and the Monte Carlo sampling simulation method for CDD are studied, and the safety evaluation method for the bearing wear life is proposed using a reliability index regarding the failure probability of monitored CBT over the wear limit in the service lifetime. The main conclusions are drawn as follows:

(1) Through monitored data analysis, the monitored longitudinal displacement data mainly consist of temperature-induced static displacements and train-induced dynamic displacements. The wavelet packet decomposition method can effectively extract the small-amplitude dynamic displacements caused by train loads from the monitored data. All the CDDs contain uniform and random characteristics, and all the CBTs have an obvious linear correlation with the number of passed trains, but their linear growth rates are different.

(2) Through probability statistics analysis, GEVD can well describe the cumulative probability characteristics of CDD. The Monte Carlo sampling simulation was performed using GEVD to simulate CDD and CBT, and the results show that the simulated cumulative probabilities of CDD have agreement with the monitored ones of CDD, and the simulated linear growth rates of CBT have agreement with the monitored ones of CBT.

(3) Through safety evaluation analysis, the safety evaluation method for the bearing wear life is proposed using a reliability index, and it is finally judged whether the CBTs can exceed the wear limit in the service lifetime. The evaluation results show that all the spherical steel bearings do not exceed the wear limit in the service life.

Notation

$B_{i,u}$: ith spherical steel bearing at the upstream
$B_{i,d}$: ith spherical steel bearing at the downstream
CBT: cumulative bearing travel
CDD: cumulative dynamic displacement
CP: cumulative probability
$D_{i,u}$: monitored longitudinal displacement data at the ith spherical steel bearing $B_{i,u}$
$D_{i,d}$: monitored longitudinal displacement data at the ith spherical steel bearing $B_{i,d}$
$\tilde{D}(k)$: dynamic displacement caused by the kth passed train

$\tilde{D}_j(k)$: jth value in $\tilde{D}(k)$
$F([M_{i,\mathrm{us}}])$: cumulative distribution function with assigned value $[M_{i,\mathrm{us}}]$
$F([M_{i,\mathrm{ds}}])$: cumulative distribution function with assigned value $[M_{i,\mathrm{ds}}]$
GEVD: general extreme value distribution
$G(N_{i,\mathrm{u}})$: cumulative distribution function of $N_{i,\mathrm{u}}$
$G(N_{i,\mathrm{d}})$: cumulative distribution function of $N_{i,\mathrm{d}}$
$G(N_{i,\mathrm{us}})$: cumulative distribution function of $N_{i,\mathrm{us}}$
$G(N_{i,\mathrm{ds}})$: cumulative distribution function of $N_{i,\mathrm{ds}}$
LVDT: linear variable differential transformer
$\mathrm{mean}(N_{i,\mathrm{u}})$: average value of 3495 CDDs for each $N_{i,\mathrm{u}}$
$\mathrm{mean}(N_{i,\mathrm{d}})$: average value of 3495 CDDs for each $N_{i,\mathrm{d}}$
$M(p)$: CBT caused by p passed trains
$M_{i,\mathrm{u}}$: CBT of $B_{i,\mathrm{u}}$
$M_{i,\mathrm{d}}$: CBT of $B_{i,\mathrm{d}}$
$[M_{i,\mathrm{us}}]$: wear limit of $B_{i,\mathrm{u}}$
$[M_{i,\mathrm{ds}}]$: wear limit of $B_{i,\mathrm{d}}$
$N(k)$: cumulative travel of bearing caused by the kth passed train
$N_{i,\mathrm{u}}$: set of $\{N(1), N(2), \ldots, N(3495)\}$ for the bearings $B_{i,u}$
$N_{i,\mathrm{d}}$: set of $\{N(1), N(2), \ldots, N(3495)\}$ for the bearings $B_{i,\mathrm{d}}$
$N_{i,\mathrm{us}}$: simulated CDDs of $N_{i,\mathrm{u}}$
$N_{i,\mathrm{ds}}$: simulated CDDs of $N_{i,\mathrm{d}}$
$\mathrm{NUM}(N_{i,\mathrm{u}})$: total number of $N_{i,\mathrm{u}}$
$\mathrm{NUM}(N_{i.\mathrm{d}})$: total number of $N_{i,\mathrm{d}}$
$\mathrm{NUM}(N_{i,u} < N_{i,\mathrm{u}}(j))$: number of CDDs in $N_{i,\mathrm{u}}$ that are smaller than $N_{i,\mathrm{u}}(j)$
$\mathrm{NUM}(N_{i,\mathrm{d}} < N_{i,\mathrm{d}}(j))$: number of CDDs in $N_{i,\mathrm{d}}$ that are smaller than $N_{i,\mathrm{d}}(j)$
ND: normal distribution
PTFE: poly-tetra-fluoro-ethylene
$P(N_{i,\mathrm{u}}(j))$: CP of the jth value $N_{i,\mathrm{u}}(j)$ in $N_{i,\mathrm{u}}$
$P(N_{i,\mathrm{d}}(j))$: CP of the jth value $N_{i,\mathrm{d}}(j)$ in $N_{i,\mathrm{d}}$
P_{f}: failure probability
R: value of cumulative probability
WD: Weibull distribution
$x_{j,m}$: wavelet packet coefficient in the mth frequency band of the jth scale
$[\beta]$: target reliability level.

Data Availability

The data used to support the findings of this study are available from the corresponding author upon request.

Conflicts of Interest

The authors declare that they have no conflicts of interest.

Acknowledgments

The authors thank the Natural Science Foundation of Jiangsu Province of China (BK20180652) and the China Postdoctoral Science Foundation (2017M621865).

References

[1] J. W. Zhan, H. Xia, N. Zhang, and Y. Lu, "A diagnosis method for bridge rubber support disease based on impact responses," *Journal of Vibration and Shock*, vol. 32, no. 8, pp. 153–157, 2013, in Chinese.

[2] B. Wei, T. H. Yang, L. Z. Jiang, and X. H. He, "Effects of friction-based fixed bearings on the seismic vulnerability of a high-speed railway continuous bridge," *Advances in Structural Engineering*, vol. 21, no. 5, pp. 643–657, 2018.

[3] J. Oh, C. Jang, and J. H. Kim, "A study on the characteristics of bridge bearings behavior by finite element analysis and model test," *Journal of Vibroengineering*, vol. 17, no. 5, pp. 2559–2571, 2015.

[4] J. J. Huang, Q. Su, L. C. Zhang, Y. J. Li, and B. Liu, "Rapid treatment technique of diseases of the rocking axle bearing of railway simply supported beam bridge," *Applied Mechanics and Materials*, vol. 351-352, pp. 1440–1444, 2013.

[5] A. S. Deshpande and J. M. C. Kishen, "Fatigue crack propagation in rocker and roller-rocker bearings of railway steel bridges," *Engineering Fracture Mechanics*, vol. 77, no. 9, pp. 1454–1466, 2010.

[6] Q. J. Shi, "Defect analysis and reconstruction method for existing railway bridge bearing," *Railway Engineering*, vol. 57, no. 10, pp. 12–14, 2017.

[7] S. Y. Yan, "An analysis of causes for defects of roller bearing and treatment measures," *Railway Standard Design*, vol. 2002, no. 6, pp. 30–32, 2002, in Chinese.

[8] H. Wang, *Study on Damage Identification Method for Railway Bridge Rubber Bearings Based on Dynamic Responses*, Beijing Jiaotong University, Beijing, China, 2014, in Chinese.

[9] Z. Qiao, *Study on the Bridge Bearing Disease Identification Technique Based on the Natural Frequency Change Rate*, East China Jiaotong University, Nanchang, China, 2014, in Chinese.

[10] S. L. Chen, Y. Q. Liu, and Y. B. Zhang, "Effects of bearing damage on vibration characteristics of a large span steel truss bridge," *Journal of Vibration and Shock*, vol. 36, no. 13, pp. 195–200, 2017, in Chinese.

[11] F. Q. Hu, J. Chen, Y. B. Xu, and X. M. Feng, "Analysis of mechanical properties of continuous T-beam bridge with diseased bearings," *Journal of Nanchang University Engineering and Technology*, vol. 37, no. 2, pp. 123–127, 2015, in Chinese.

[12] H. Zhou, K. Liu, G. Shi, Y. Q. Wang, Y. J. Shi, and G. De Roeck, "Fatigue assessment of a composite railway bridge for high speed trains. Part I: modeling and fatigue critical details," *Journal of Constructional Steel Research*, vol. 82, pp. 234–245, 2013.

[13] T. Guo, J. Liu, and L. Y. Huang, "Investigation and control of excessive cumulative girder movements of long-span steel suspension bridges," *Engineering Structures*, vol. 125, pp. 217–226, 2016.

[14] T. Guo, J. Liu, Y. F. Zhang, and S. J. Pan, "Displacement monitoring and analysis of expansion joints of long-span steel bridges with viscous dampers," *Journal of Bridge Engineering*, vol. 20, no. 9, article 04014099, 2015.

[15] Y. L. Ding and G. X. Wang, "Evaluation of dynamic load factors for a high-speed railway truss arch bridge," *Shock and Vibration*, vol. 2016, Article ID 5310769, 15 pages, 2016.

[16] G. X. Wang, Y. L. Ding, Y. S. Song, L. Y. Wu, Q. Yue, and G. H. Mao, "Detection and location of the degraded bearings based on monitoring the longitudinal expansion performance of the main girder of the Dashengguan Yangtze Bridge," *Journal of Performance of Constructed Facilities*, vol. 30, no. 4, article 04015074, 2016.

[17] G. X. Wang and Y. L. Ding, "Research on monitoring temperature difference from cross sections of steel truss arch girder of Dashengguan Yangtze Bridge," *International Journal of Steel Structures*, vol. 15, no. 3, pp. 647–660, 2015.

[18] M. Y. Gokhale and K. D. Kaur., "Time domain signal analysis using wavelet packet decomposition approach," *International Journal of communications Networks and System Sciences*, vol. 3, no. 3, pp. 321–329, 2010.

[19] T. Figlus, S. Liscak, A. Wilk, and B. Aazarz, "Condition monitoring of engine timing system by using wavelet packet decomposition of a acoustic signal," *Journal of Mechanical Science and Technology*, vol. 28, no. 5, pp. 1663–1671, 2014.

[20] R. Wald, T. M. Khoshgoftaar, and J. C. Sloan, "Feature selection for optimization of wavelet packet decomposition in reliability analysis of systems," *International Journal on Artificial Intelligence Tools*, vol. 22, no. 5, article 1360011, 2013.

[21] EN 1991-1-5, *Eurocode 1: Actions on Structures—Part 1–5: General Actions—Thermal Actions*, European Committee for Standardization (CEN), Brussels, Belgium, Europe, 2004.

[22] P. Kotes and J. Vican, "Reliability levels for existing bridges evaluation according to eurocodes," *Procedia Engineering*, vol. 40, pp. 211–216, 2012.

[23] TB/T 3320-2013, *Spherical Bearings for Railway Bridges*, China Railway Publishing House, Beijing, China, 2013, in Chinese.

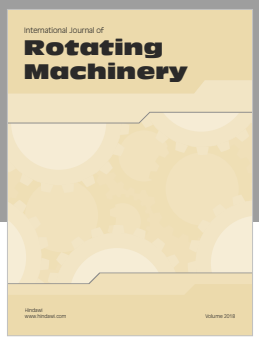

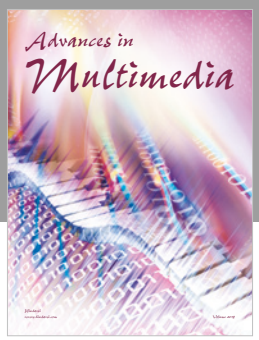

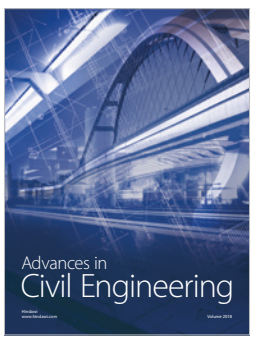

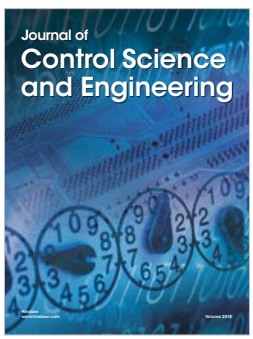

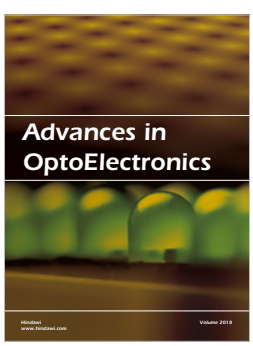

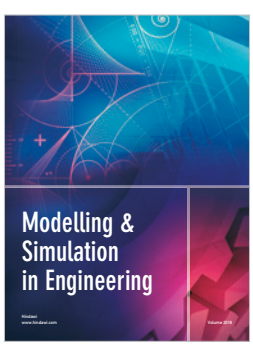

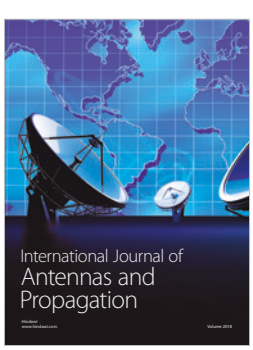

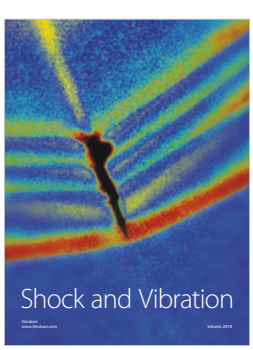

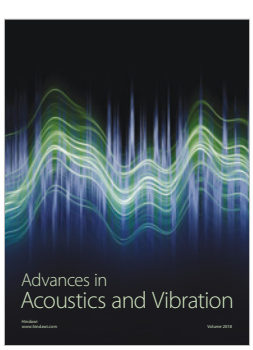

Hindawi

Submit your manuscripts at
www.hindawi.com